

## Current Dependence Growth of ZnO Nanostructures by Electrochemical Deposition Technique

N. K. Hassan<sup>1</sup>, M. R. Hashim<sup>1,\*</sup>, Y. Al-Douri<sup>2</sup>, K. Al-Heuseen<sup>3</sup>

<sup>1</sup> School of Physics, Universiti Sains Malaysia, 11800-Penang, Malaysia

<sup>2</sup> Institute of Nano Electronic Engineering, University Malaysia Perlis, 01000 Kangar, Perlis, Malaysia

<sup>3</sup> Al-Balqa Applied University, Ajloun University College, Jordan

\*E-mail: [roslan@usm.my](mailto:roslan@usm.my)

Received: 26 March 2012 / Accepted: 14 April 2012 / Published: 1 May 2012

---

Zinc oxide (ZnO) nanostructure with a hexagonal structure is deposited on Si (100) substrates through electrochemical deposition (ECD) using a current density of 2, 3, and 4 mA/cm<sup>2</sup> for 1.5 h. The photoluminescence (PL) intensity of the films has large peaks around the ultraviolet and green emission. The green emission may correspond to the electron transition from the defects to the valence band. The intensity of these two emissions changes with respect to the current density. X-ray diffraction (XRD) measurements show that the peaks of these grown samples refer to the ZnO with a hexagonal structure and a preferable orientation of (101). Refractive index, optical dielectric constant, and bulk modulus are investigated in the ZnO nanostructure. The obtained results are in good agreement with the experimental and theoretical ones.

---

**Keywords:** ZnO; Nanostructure; Electrochemical deposition; Refractive index; Bulk modulus.

### 1. INTRODUCTION

Zinc oxide (ZnO) semiconductors have a promising future. With their wide, direct bandgap (3.37 eV) and large exciton binding energy (60 meV) at room temperature, ZnO semiconductors have a broad range of applications, particularly in light-emitting diodes, photo detectors, and gas sensors [1–3]. These semiconductors also have a stable wurtzite structure with lattice spacing of  $a = 0.325$  nm and  $c = 0.521$  nm. ZnO has a strong emission even at room temperature. Therefore, the high-efficiency detection of ultraviolet (UV) emissions is possible using ZnO-based optical devices [4].

A variety of approaches have been employed for producing ZnO nanostructures, such as chemical vapor deposition, thermal evaporation, and pulsed laser deposition [5–7]. In the development

of ZnO-based optical devices, the search for effective low-cost techniques has led to a chemical-related method called electrochemical deposition (ECD) [8, 9]. ECD differs from other methods as follows: the thickness and surface morphology can be controlled by growth parameters; the deposition rate is relatively high; the experimental setup is low cost; the processing temperature is low; and the ease of impurity doping is evident [10–12]. Yang et al. [13] reported the effect of zinc nitrate concentration on the structural and optical properties of ZnO. The surface condition of the substrate effect on the formation of ZnO was studied by Yiwen Tang et al. [14] using three-electrode electrochemical cells.

The present work reports the influence of the current density on the structural and optical properties of ZnO nanostructures grown on Si (100) substrates using the ECD technique. Structural and optical properties of the samples were measured using scanning electron microscopy (SEM), X-ray diffraction (XRD), and photoluminescence (PL) measurements, and were investigated theoretically using specific models of the ZnO nanostructure. The effects of the current density on both structural and optical properties were discussed.

## 2. EXPERIMENTAL PROCEDURE

The ZnO nanostructure was deposited by ECD technique through Zn (NO<sub>3</sub>)<sub>2</sub> aqueous solutions at room temperature. Using a simple two-electrode homemade Teflon cell, a spiral platinum wire was used as the anode and the Si (100) substrate as the cathode. The distance between the electrodes was about 0.5 cm. Electrodeposition was carried out by changing the current density between 2, 3, and 4 mA/cm<sup>2</sup>. The pH was adjusted to 5, and the deposition time was 1.5 h. All the products of ZnO film were then annealed at 500 °C under oxygen ambient. The synthesized products were characterized using XRD, PAN alytical X'Pert PRO diffractometer with Cu K $\alpha$  radiation, and SEM model JEOL JSM-6460LV with energy dispersive X-ray spectroscopy EDX installed. The PL spectra of the samples were measured using He-Cd laser (325 nm) at room temperature.

## 3. RESULTS AND DISCUSSION

### 3.1 Morphology of ZnO films

The SEM images of the ZnO nanostructure deposited on Si (100) using different current densities of 2, 3, and 4 mA/cm<sup>2</sup> for 1.5 h. and annealed at 500 °C. with EDX spectrum of the film deposited by ECD are shown in (Fig. 1). The surface morphology of the ZnO sample deposited at 2 mA/cm<sup>2</sup> shows a particle-like structures grew onto the surface, these particles superimposed on each other's Fig.1 (a). Moreover, they are in a different direction with their tips and are deposited to be set up with no uniform shape. When the current density applied on the cell is increased to 3 mA/cm<sup>2</sup>, the Zn<sup>+2</sup> separates from the zinc nitrate under the influence of the applied electric field to the cell. It moves to the cathode faster than the previous sample and will melt in water. The latter will then bond with oxygen to make ZnO particles, which are arranged as pyramids distributed in a uniform and compact

manner. Increasing the current density to  $4 \text{ mA/cm}^2$   $\text{Zn}^{+2}$  will separate faster, leading to more  $\text{Zn}^{+2}$  ions than oxygen. With the shapes of the pyramids destroyed,  $\text{ZnO}$  particles with irregular shapes and a much less compact structure [Fig. 1(c)] than the previous two samples emerge. The EDX image shows that the rate of the  $\text{ZnO}$  film deposition is considered that of the rate of Zn to O, which is different in all samples, thereby affecting the optical properties of the films.

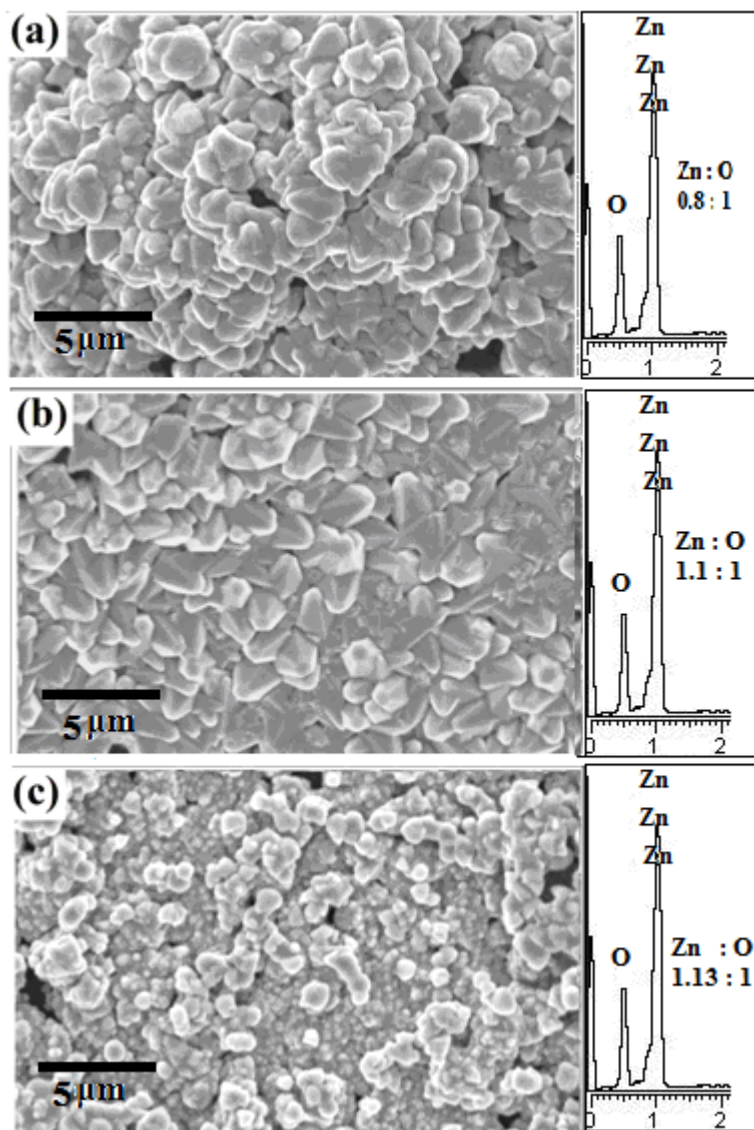
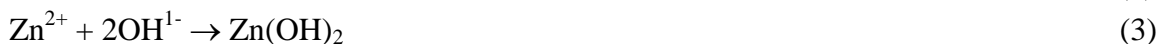


**Figure 1.** SEM images and EDX spectra of  $\text{ZnO}$  films using different current densities: (a) 2, (b) 3, and (c)  $4 \text{ mA/cm}^2$

When  $\text{Zn}(\text{NO}_3)_2$  melts in water, the possible reactions that take place in the cell under the applied electric field can be written as follows:





### 3.2 Optical properties of ZnO nanostructure

The PL spectra of the ZnO nanostructure deposited on Si (100) at room temperature are shown in Fig. 2.

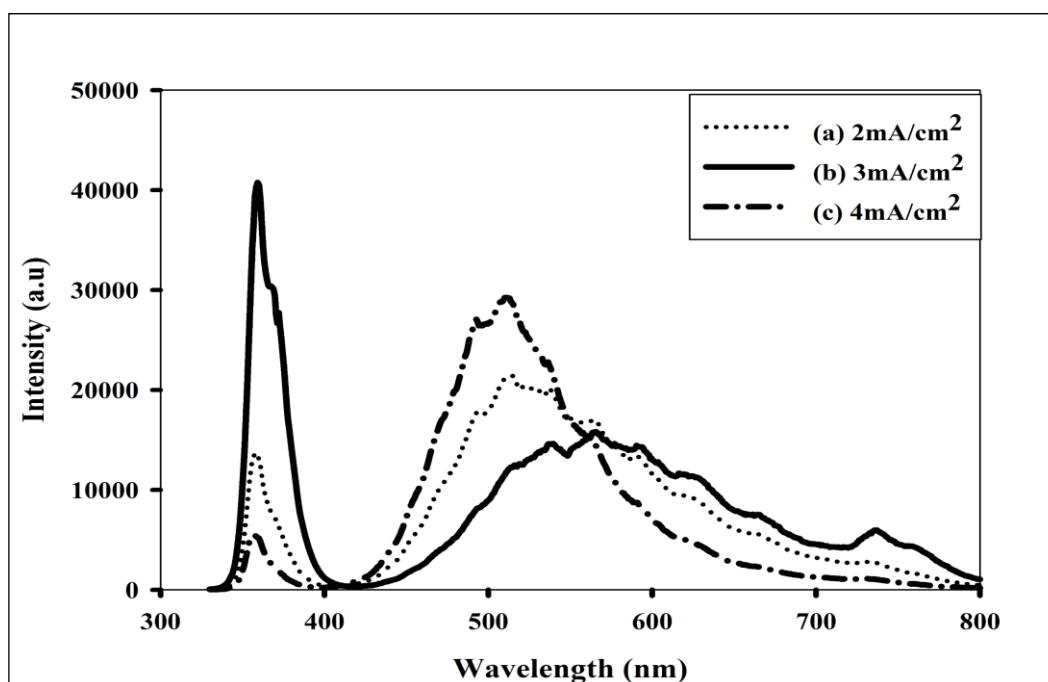


**Figure 2.** PL spectra of ZnO films using different current densities: (a) 2, (b) 3, and (c) 4 mA/cm<sup>2</sup>

All samples grown using ECD have a two-peak PL spectra: toward the UV and around the green emission. The sample grown at 3 mA/cm<sup>2</sup> shows the highest UV intensity and the lowest green emission, whereas the other, which is grown at 4 mA/cm<sup>2</sup> shows the lowest UV intensity and the highest green emission. The peak wavelengths for the near-band-edge UV emission are 358, 360, and 356 nm for the samples deposited at 2, 3, and 4 mA/cm<sup>2</sup>, respectively. These peaks are generated by the recombination of the excitons through an exciton–exciton collision process [15]. The spectra were observed to be slightly blue-shifted in the samples deposited with 2 and 4 mA/cm<sup>2</sup> compared with the sample of 3 mA/cm<sup>2</sup>, this phenomenon indicates that the compressive stress takes place in these two samples. The appearance of the blue-shifted PL emission may be correlated with the development of highly anisotropic structures in the morphology. Based on available literature, many defects related to the PL spectra have been reported [16]. The reason for the presence of this peak may be related to the

exciton that is bound to structural defects, strain-induced structural defects, incorporation of impurity-induced disorder, or surface defects during growth process.

The narrow peak at 360 nm with a high intensity of near-band-edge emission as well as the decrease in the peak of green emission observed in Fig. 2(b) resulted from high crystallization. Bagnall et al. [17] demonstrated that the improvement of crystal quality could cause a high-intensity near-band-edge emission with very low or no green emission [17]. This finding indicates that the ZnO grown at 3 mA/cm<sup>2</sup> has the best crystallization. As for the green emission that is related to sub-band transition, the peak wavelengths are about 513, 533, and 507 nm for the samples deposited at 2, 3, and 4 mA/cm<sup>2</sup>, respectively. This band may be related to the defects in the samples, including vacancies, interstitials, and antisites. Therefore, the difference in the intensity of the peak indicates that the level of defects in the samples is responsible for the recombination of the green luminescence. The sample deposited at 3 mA/cm<sup>2</sup> shows that the lowest intensity suggests the lowest level of defects, whereas the sample deposited at 4 mA/cm<sup>2</sup> shows that the highest intensity suggests the highest level of defect. These results are consistent with the SEM images in Fig. 1.

A broad green emission from the ZnO nanostructure stronger than the UV emission can be observed in the ZnO samples grown at a current density of 2 and 4 mA/cm<sup>2</sup>. This finding is related to the high quantity of the surface oxygen vacancies and defects of the ZnO, such as Zn vacancy ( $V_{Zn}$ ). An oxygen vacancy has three possible charge states: neutral oxygen vacancy ( $VO^0$ ), singly ionized oxygen vacancy ( $VO^+$ ), and doubly ionized oxygen vacancy ( $VO^{++}$ ). The oxygen singly ionized state is unstable, and the transition involving it can be seen as a red emission in PL. Therefore, oxygen vacancies are either in the neutral or doubly charged state.

The sample deposited at 2 mA/cm<sup>2</sup> as (EDX) confirms that the element ratio of Zn:O indicates that this sample is O-rich. Therefore, the main point of defects should be the Zn vacancy ( $V_{Zn}$ ) defects. The EDX inset (Fig. 1) shows that the element ratio of Zn:O changes with the other two samples by increasing the current density, indicating that the Zn ion transfer becomes faster. and that the rate of Zn atoms compound with oxygen in obtaining pure ZnO increases with the current density of 3 mA/cm<sup>2</sup>. As the current density increases, Zn atoms also increase as a result of the fast-moving Zn ions. Zn atoms are diffused to remain at the interstitial sites and act as shallow donors. This ratio indicates that the green luminescence in the samples is deposited at 4 mA/cm<sup>2</sup> because of the oxygen vacancies. Based on this discussion, reducing the defects by choosing an appropriate current density is possible, leading to a reduction of green emission.

The refractive index  $n$  is a very important physical parameter related to the microscopic atomic interactions. From a theoretical viewpoint, there are two different approaches to this subject: the relation between the refractive index and the density, and the local polarizability of these entities [18]. Consequently, many attempts have been made to relate the refractive index to the energy gap  $E_g$  through simple relationships [19–24]. However, these relations of  $n$  are independent of temperature and incident photon energy. The various relations between  $n$  and  $E_g$  are reviewed in the current paper. Ravindra et al. [24] presented a linear form of  $n$  as a function of  $E_g$ :

$$n = \alpha + \beta E_g \quad (5)$$

where  $\alpha = 4.048$  and  $\beta = -0.62 \text{ eV}^{-1}$ . Light refraction and dispersion are inspired. Herve and Vandamme [25] proposed an empirical relation as follows:

$$n = \sqrt{1 + \left( \frac{A}{E_g + B} \right)^2} \tag{6}$$

where  $A = 13.6 \text{ eV}$  and  $B = 3.4 \text{ eV}$ . As regards group IV semiconductors, Ghosh et al. [26] found an empirical relationship based on the band structure and quantum dielectric considerations of Penn [27] and Van Vechten [28]:

$$n^2 - 1 = \frac{A}{(E_g + B)^2} \tag{7}$$

where  $A = 8.2E_g + 134$ ,  $B = 0.225E_g + 2.25$ , and  $(E_g + B)$  refers to an appropriate average energy gap of the material. The calculated refractive indices of the end-point compounds are listed in Table 1.

**Table 1.** Calculated refractive indices of ZnO films under different current densities using Ravindra et al. [24], Herve and Vandamme [25], and Ghosh et al. [26] models corresponding to the optical dielectric constant

Current density (mA/cm <sup>2</sup> )	$n$	$\epsilon_\infty$
0	2.064 <sup>a</sup> 2.290 <sup>b</sup> 2.329 <sup>c</sup> 2.008 <sup>d</sup>	4.260 <sup>a</sup> 5.244 <sup>b</sup> 5.424 <sup>c</sup>
2	1.902 <sup>a</sup> 2.220 <sup>b</sup> 2.278 <sup>c</sup>	3.617 <sup>a</sup> 4.928 <sup>b</sup> 5.189 <sup>c</sup>
3	1.915 <sup>a</sup> 2.225 <sup>b</sup> 2.282 <sup>c</sup>	3.667 <sup>a</sup> 4.950 <sup>b</sup> 5.207 <sup>c</sup>
4	1.890 <sup>a</sup> 2.215 <sup>b</sup> 2.275 <sup>c</sup>	3.572 <sup>a</sup> 4.906 <sup>b</sup> 5.175 <sup>c</sup>

<sup>a</sup>Ref. [24], <sup>b</sup>Ref. [25], <sup>c</sup>Ref. [26], <sup>d</sup>Ref. [29] Exp.

This relationship is verified by the calculation of the optical dielectric constant  $\epsilon_\infty$ , which depends on the refractive index. Note that  $\epsilon_\infty = n^2$  [30]. The investigated refractive indices  $n$  are clearly in agreement with the experimental value [29], and the model of Ravindra et al. [24] agrees well for ZnO films in enhancing the photo conversion. The high absorption and low reflection may be attributed to the increase in efficiency of optoelectronic devices.

### 3.3 Structural properties of ZnO nanostructure

The typical XRD pattern of a ZnO nanostructure deposited on Si (100) by ECD technique at different current densities reveals seven peaks, as shown in Fig. 3. All the samples showed similar

XRD patterns that demonstrate high-crystalline hexagonal wurtzite structures of ZnO. The diffraction peaks are sharp and have a high intensity, indicating that the samples are highly crystalline in terms of their ZnO nanostructure.

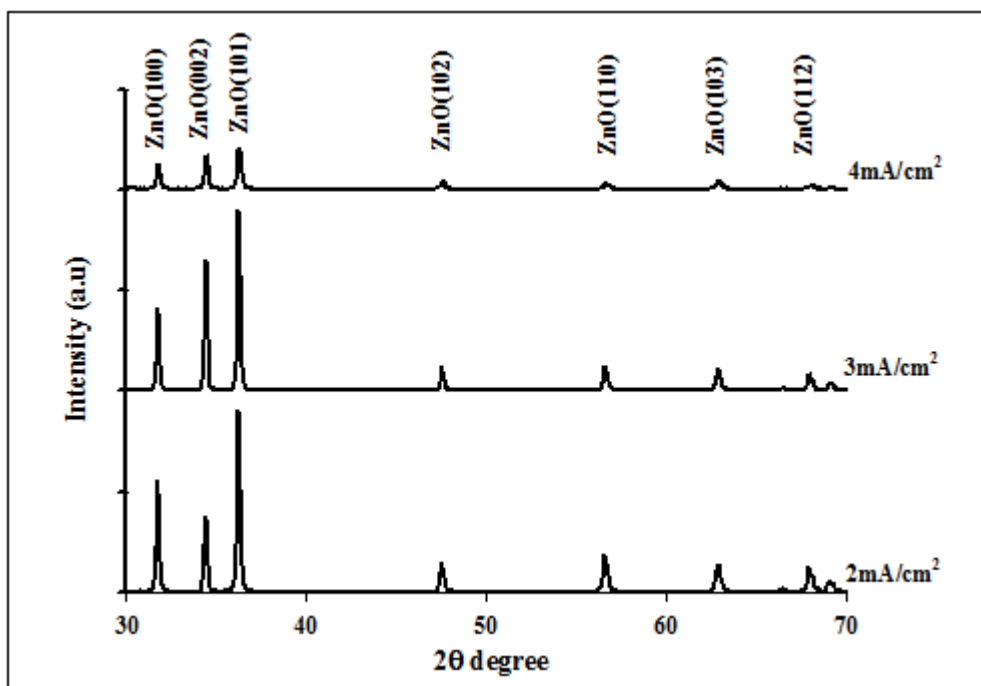


**Figure 3.** XRD spectrum of ZnO films grown at various current densities: (a) 2, (b) 3, and (c) 4 mA/cm<sup>2</sup>

The sample deposited at 2 mA/cm<sup>2</sup> [Fig. 3(a)] shows the ZnO epitaxially grown on the Si (100) substrate. This growth can be observed from the presence of the peaks at 31.73, 34.40, 36.23, 47.53, 56.58, 62.86, and 67.92, which correspond to (100), (002), (101), (102), (110), (103), and (112) orientations, respectively. As shown in the XRD data, the (101) direction in Fig. 3 is the preferred orientation for the three samples. The peak intensity of this orientation increased and became narrow for the sample grown at 3 mA/cm<sup>2</sup>. At the same time, the peak intensity of the (100) orientation was higher than that of the (002) orientation for the sample grown at 2 mA/cm<sup>2</sup>, which underwent reorientation. However, the peak intensity of the (002) orientation was higher in the other samples, indicating that the *c*-axis orientation significantly improved, as seen in Figs. 3b and c.

The bulk modulus denotes material stiffness, a property important in different industries. Many researchers [31–36] have made various efforts to explore the thermodynamic properties of solids. In these studies, the thermodynamic properties were studied, such as the inter-atomic separation and bulk modulus of solids with different approximations and best-fit relations [33–36]. Computing with great accuracy is now possible using a significant number of structural and electronic properties of solids. The *ab initio* calculations are complex and require significant effort. Therefore, more empirical approaches have been developed [37, 38] to compute the properties of materials. In many cases, the empirical methods offer the advantage of applicability to a broad class of materials and illustrating

trends. In many applications, these empirical approaches do not give highly accurate results for each specific material, but they are still very useful. Cohen [39] established an empirical formula for the calculation of bulk modulus  $B_0$ , which is based on the nearest-neighbor distance. His result agrees with the experimental values. Lam et al. [40] derived an analytical expression for the bulk modulus from the total energy. This expression is different in structure from the empirical formula but gives similar numerical results. They also obtained an analytical expression for the pressure derivative  $B_0$  of the bulk modulus. Our group [41] used a concept based on the lattice constant to establish an empirical formula for the calculation of the bulk modulus. The calculated results agree with the experimental data and other calculations. The hypothetical structure and simulation of the experimental conditions are required to use this formula practically.

The dominant effect is the degree of covalency characterized by Phillips' homopolar gap  $E_h$  [37], which shows how a qualitative concept such as the bulk modulus can be related to the lattice constant. One reason for presenting these data in the current work is that the validity of our calculations is not restricted in a computed space. Thus, we believe that the data will prove valuable in future research in this field.

An important reason for studying  $B_0$  is the observation of clear differences between the lattice constants for different ZnO samples, as seen in Table 2.

**Table 2.** Energy gaps (eV), lattice constants (Å), and bulk modulus (GPa) of ZnO films under different current densities along with theoretical [42, 43] and experimental data [44]

Current density (mA/cm <sup>2</sup> )	Energy gap (eV)	a=b (Å)	c (Å)	B0 (GPa)
0	3.2	3.2499*	5.2068*	128.26\$
		3.249a	5.2048a	166a
				156.30b
				183c
2	3.46	3.2530*	5.2130*	510.233\$
3	3.44	3.2501*	5.2071*	511.828\$
4	3.48	3.2488*	5.2054*	512.545\$

\*Measured value, \$Calculated value, <sup>a</sup>Ref. [42] Theor., <sup>b</sup>Ref. [43] Theor., <sup>c</sup>Ref. [44] Exp.

The basis of our model is the lattice constant presented in Table 2. The fitting of these data gives the following empirical formula [41]:

$$B_0 = [3000 - 100\lambda] \left( \frac{a}{2} \right)^{-3.5} \tag{8}$$

where  $a$  is the lattice constant (in Å), and  $\lambda$  is an empirical parameter accounting for the effect of ionicity;  $\lambda = 0; 1, 2$  for groups IV, III–V, and II–VI semiconductors, respectively. In Table 2, the

calculated bulk moduli values are compared with the theoretical [42, 43] and experimental [44] values fitted in Fig. 4. The bulk modulus of the ZnO nanostructure increases as the current density increases, including the attributes of the nanostructure.

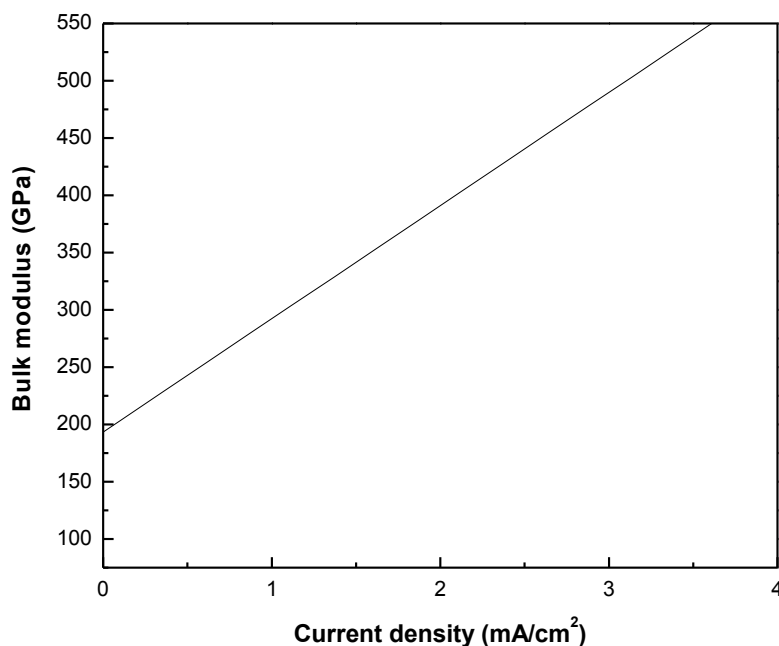


**Figure 4.** Fitted variation of bulk moduli for ZnO as a function of current densities

We can conclude that the calculated bulk modulus is in accordance with the other results [42–44]. These studies exhibit the same chemical trends as those found in the values derived from the experimental values, as shown in Table 2. The calculated bulk modulus agrees well with the other data.

#### 4. CONCLUSION

ZnO nanostructure was synthesized using the ECD technique. The optical properties were measured, revealing that the energy band gap depends on the growth parameters and current density. The defects in the ZnO nanostructure obtained in the samples deposited at low and high current densities are considered the main reason for the green emission in PL. The defects can be reduced by choosing an appropriate current density, as this parameter affects the structural properties. High-crystalline ZnO was then obtained by controlling the current density. The current density of 3 mA/cm<sup>2</sup> gave the best crystallization and high intensity. The obtained results of the refractive index, optical dielectric constant, and bulk modulus suggest that the ZnO nanostructure is more suitable for highly sensitive devices and that Ravindra et al.'s model is a more appropriate model to explain our experimental results.

**References**

1. P.A. Savariumuthu, I.L. Jeong, K.K. Jin, *Appl. Phys. Lett.* 90 (2007) 103
2. N. Saito, H. Haneda, T. Sekiguchi, N. Ohashi, I. Sakaguchi, K. Koumoto, *Adv. Mater.* 14 (2002) 418
3. N. Ohashi, K. Kataoka, T. Ohgaki, T. Miyagi, H. Haneda, K. Morinaga, *Appl. Phys. Lett.* 83 (2003) 4857
4. T. Pauporte, D. Lincot, *Electrochim. Acta* 45 (2000) 3345
5. W.I. Park, D.H. Kim, S.W. Jung, G.C. Yi, *Appl. Phys. Lett.* 80 (2002) 4232
6. X.H. Kong, X.M. Sun, X.L. Li, Y.D. Li, *Mater. Chem. Phys.* 82 (2003) 997
7. J. Zuniga-Perez, A. Rahm, C. Czekalla, J. Lenzner, M. Lorenz, M. Grundmann, *Nanotechnology* 18 (2007) 195303
8. K. Al-Heuseen, M.R. Hashim, N.K. Ali, *Mater. Lett.* 64 (2010) 1604
9. J. Katayama, M. Izaki, *J. Appl. Electrochem.* 30 (2000) 855
10. Y.F. Gao, M. Nagai, Y. Masuda, F. Sato, K.J. Kuomoto, *Cryst. Grow.* 286 (2006) 445
11. Z.H. Gu, T.Z. Fahidy, *J. Electrochem. Dep.* 146 (1999) 156
12. Z.G. Chen, Y.W. Tang, L.S. Zhang, L.J. Luo, *Electrochim. Acta* 51 (2006) 5870
13. Hee Yeon Yang, Se Han Lee, Tae Whan Kim, *Appl. Sur. Sci.* 256 (2010) 117
14. Yiwen Tang et al, *Electrochemistry Communi.* 9 (2007) 289
15. K. Vanheusden, C.H. Seager, W.L. Warren, D.R. Tallant, J.A. Voigt, *J. Appl. Phys.* 79 (1996) 7983
16. M. A. Reshchikov, H. Morkoc, *J. Appl. Phys.* 97 (2005) 061301
17. D.M. Bagnall, Y.F. Chen, Z. Zhu, T. Yao, S. Koyama, M.Y. Shen, T. Goto, *Appl. Phys. Lett.* 73 (1998) 1038
18. N. M. Balzaretti, J.A.H. da Jornada, *Solid State Commun.* 99 (1996) 943
19. T. S. Moss, *Proc. Phys. Soc. B*, 63 (1950) 167
20. V. P. Gupta, N.M. Ravindra, *Phys. Stat. Sol. B*, 100 (1980) 715
21. Y. Al-Douri, Y. P. Feng, A.C.H. Huan, *Solid State Commun.* 148 (2008) 521
22. Y. Al-Douri, A. H. Reshak, H. Baaziz, Z. Charifi, R. Khenata, S. Ahmad, U. Hashim, *Solar Energy* 84 (2010) 1979
23. P. Herve, L. K. J. Vandamme, *Infrared Phys. Technol.* 35 (1993) 609
24. N. M. Ravindra, S. Auluck, V.K. Srivastava, *Phys. Stat. Sol. (b)* 93 (1979) K155
25. P. J. L. Herve, L. K. J. Vandamme, *J. Appl. Phys.* 77 (1995) 5476
26. D. K. Ghosh, L.K. Samanta, G.C. Bhar, *Infrared Phys.* 24 (1984) 34
27. D. R. Penn, *Phys. Rev.* 128 (1962) 2093
28. J. A. Van Vechten, *Phys. Rev.* 182 (1969) 891
29. Handbook of Chemistry & Physics, 53th Edition, CRC Press, USA, (1973)
30. G. A. Samara, *Phys. Rev. B*, 27 (1983) 3494
31. A. M. Sherry, M. Kumar, *J. Phys. Chem. Solids* 52 (1991) 1145
32. J. L. Tallon, *J. Phys. Chem. Solids* 41 (1980) 837
33. M. Kumar, S.P. Upadhyaya, *Phys. Stat. Sol. (b)* 181 (1994) 55
34. M. Kumar, *Physica B* 205 (1995) 175
35. R. K. Pandey, *J. Phys. Chem. Solids* 59 (1998) 1157
36. Q. He, Z-T. Yan, *Phys. Stat. Sol. (b)* 223 (2001) 767
37. J. C. Phillips, *Bonds and Bands in Semiconductors*, Academic Press, San Diego, 1973
38. W. A. Harison, *Electronic Structure and the Properties of Solids*, General Publishing Company, Toronto, 1989
39. M. L. Cohen, *Phys. Rev. B* 32 (1985) 7988
40. P. K. Lam, M.L. Cohen, G. Martinez, *Phys. Rev. B* 35 (1987) 9190
41. Y. Al-Douri, H. Abid, H. Aourag, *Mater. Chem. Phys.* 87 (2004) 14
42. Y. Z. Zhu, G. D. Chen, H. Ye, A. Walsh, C. Y. Moon, S-H. Wei, *Phys. Rev. B* 77 (2008) 245209

43. Z. Charifi, H. Baaziz, A. H. Reshak, *Phys. Stat. Sol. (b)* 244 (2007) 3154  
44. H. Karzel, W. Potzel, M. Kofferlein, W. Schiessl, M. Steiner, U. Hiller, G. M. Kalvius, D. W. Mitchell, T. P. Das, P. Blaha, K. Schwarz, M. P. Pasternak, *Phys. Rev. B* 53 (1996) 11425

© 2012 by ESG ([www.electrochemsci.org](http://www.electrochemsci.org))